Low-Dimensional Materials
https://www.sciltp.com/journals/ldm

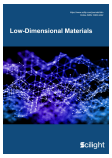

Article

Check for updates

Process for Preparing Molybdenum-Silicon Alloy Targets

Xuejia Gu [1,2,3], Ning Fan [1,2], Zhaochong Ding [1,2], Qian Jia [1,2], Yutong Ran [1,2,*] and Jinjiang He [1,2,*]

[1] Grikin Advanced Materials Co. Ltd., Beijing 102200, China
[2] National Engineering Research Center of Key Materials of Integrated Circuit, Beijing 100088, China
[3] General Research Institute for Nonferrous Metals, Beijing 100088, China
* Correspondence: ran_yutong@163.com (Y.R.); hejinjiang@grikin.com (J.H.)

How To Cite: Gu, X.; Fan, N.; Ding, Z.; et al. Process for Preparing Molybdenum-Silicon Alloy Targets. *Low-Dimensional Materials* **2026**, *2*(2), 4. https://doi.org/10.53941/ldm.2026.100004

Received: 28 April 2026
Revised: 8 June 2026
Accepted: 10 June 2026
Published: 26 June 2026

Abstract: With the development of emerging fields such as big data, artificial intelligence, and 5G communication, the critical dimensions of integrated circuits are constantly shrinking. As a high-precision tool used for pattern transfer in the lithography process, the quality of photomasks directly determines the final performance of circuits. Molybdenum silicide alloys with high silicon content have become key materials for the light-absorbing film layer in advanced photomasks due to their excellent properties such as optical tunability, ease of etching, chemical resistance, and radiation resistance. The quality of the film is highly dependent on the magnetron sputtering target material, and the development of high-uniformity and high-density molybdenum silicide alloy targets is of crucial importance. Traditional powder metallurgy methods for producing Mo-Si targets often yield compositional inhomogeneities, coarse grain structures, and cracking due to density differences between Mo and Si phases and the exothermic reaction between molybdenum and silicon. This poses significant challenges in target fabrication. This study proposes a systemic "powder pre-alloying + hot-press sintering" process. Using a mixed powder with a molybdenum-silicon atomic ratio of 1:9 as raw material, systematically investigating the effect of heat treatment temperature on molybdenum-silicon alloying. The optimal temperature was determined to be 1350 °C with a 2-h soak. The phase evolution sequence during the molybdenum-silicon reaction was elucidated as Mo + Si → Mo_3Si + Si → Mo_5Si_3 + Si → $MoSi_2$. Further investigations revealed that the resulting Si-$MoSi_2$ alloy powder exhibits brittle-brittle system characteristics. Mechanical ball milling continuously refines the particles, increasing the surface energy and density of microdefects in the powder, which helps improve the powder's sintering activity, enabling the successful production of molybdenum-silicon targets with a relative density no less than 99% and markedly improved microstructural uniformity.

Keywords: Mo-Si alloy; target; material pre-alloyed; hot-pressed sintering

1. Introduction

With the continuous development of emerging applications such as big data, artificial intelligence, 5G communications, the Internet of Things and the low-altitude economy [1,2], the critical dimensions (CD) of integrated circuits are constantly shrinking, and the precision requirements for layout design are becoming increasingly stringent. A photomask [3] serves as the master template for the patterns used in the photolithography process during integrated circuit manufacturing. It achieves the precise transfer of patterns by forming a mask pattern on a transparent substrate using an opaque light-blocking film, thereby effectively controlling the path of light. As a material used in the front-end manufacturing of integrated circuits, photomasks account for

approximately 13% of total material costs [4], and their quality directly determines the pattern accuracy and ultimate performance of the integrated circuit. To accommodate the continuous reduction in line width dimensions, photomasks have evolved from the initial Cr bipolar masks to advanced types such as phase-shift masks (PSM) and opaque MoSi bipolar masks (OMOG) [5–7]. By adjusting light transmittance, these masks continuously improve pattern resolution to achieve precise pattern transfer. Due to its excellent properties, such as optical tunability, ease of etching, and resistance to chemicals and radiation, molybdenum silicide allows for precise adjustment of optical parameters such as the refractive index n and extinction coefficient k, making it a key material for the light-absorbing thin film layers in PSM and OMOG [8,9].

Currently, magnetron sputtering [10], as a key technology for film preparation, indicates that film quality is influenced not only by the sputtering process but also by the microstructure and properties of the sputtering targets. Molybdenum-silicon alloy targets with high silicon content are the key raw materials for preparing molybdenum-silicon alloy films in mask templates via magnetron sputtering technology, and they are subject to strict requirements in terms of purity, composition, microstructural uniformity and density [11–13]. As the refractory metal molybdenum and silicon differ significantly in melting point and density, and since molybdenum-silicon alloy targets are a brittle material, conventional smelting methods struggle to achieve uniform composition and shaping; consequently, the powder metallurgy method is generally employed for their preparation [14]. Due to the substantial difference in density between the molybdenum and silicon phases, it is difficult to achieve a uniform mixture of the two. Furthermore, the exothermic reaction Mo + Si → $MoSi_2$ during sintering can cause a sudden localised rise in temperature, often resulting in coarse grain size, non-uniform distribution of composition within the target, and cracking, thereby reducing the sintering success rate [15]. By employing a powder pre-alloying process to form the Mo-Si alloy prior to sintering, the effects of the density difference between the powders and the aforementioned reaction can be mitigated [16]. In previous studies, researchers used ball milling to mechanically activate molybdenum-silicon mixed powders, yielding Mo-Si nanoactive particles, which were subsequently used to successfully synthesize tetragonal $MoSi_2$ via high-temperature self-propagating high-temperature synthesis or discharge plasma sintering. Although this process is simple and allows for pre-alloying of the powder and improved sintering activity during mechanical activation, the prolonged alloying process is prone to introducing impurities, leading to the formation of silicon oxides during subsequent sintering. In this study, high-purity molybdenum-silicon mixed powders were pre-alloyed using a heat treatment method, which not only avoids the localised temperature differences caused by the molybdenum-silicon reaction but also effectively controls the impurity content in the powder.

To improve microstructural uniformity and mitigate the effects of the exothermic Mo-Si reaction, this study utilised high-purity Mo and Si powders as raw materials. By controlling the heat treatment process of the Mo-Si mixed powder and subjecting it to subsequent ball milling, a Mo-Si alloy powder with excellent properties was prepared, which was then used to fabricate high-density Mo-Si target materials with a uniform microstructure. The study focused on the influence of heat treatment temperature on the alloying effect of molybdenum-silicon. By combining thermodynamic and kinetic behaviour, it elucidated the phase evolution process during the molybdenum-silicon reaction and analysed the relationship between the degree of consolidation of the alloy powder during comminution and its microstructure. As a result, molybdenum-silicon target materials with excellent properties were produced, providing insights into the control of microstructural uniformity in molybdenum-silicon target materials.

2. Experiment

2.1. Materials

The experiment utilised fine-grained molybdenum powder and silicon powder, both with a purity greater than 4N. The mixed powders, prepared with an atomic ratio of Mo:Si = 1:9, were thoroughly blended and vacuum-packed for later use. A small amount of the molybdenum-silicon mixed powder was subjected to differential scanning calorimetry-thermogravimetric analysis (DSC-TG). Figure 1 below shows the DSC-TG test curve of the molybdenum-silicon mixed powder, the upward and downward peaks correspond to endothermic and exothermic events in the DSC curve, respectively. The TG curve indicates that there was essentially no change in mass during the heating process. The DSC curve reveals exothermic peaks at approximately 1305 °C and 1340 °C, indicating that the heterogeneous solid-state reaction between the molybdenum and silicon components proceeds in stages, with the reaction being complete at 1361 °C. For silicon-rich molybdenum-silicon target materials, the phase composition consists of stable $MoSi_2$ and elemental Si phases. Through DSC-TG thermal analysis testing, the reaction behaviour of molybdenum and silicon, as well as the pathways of phase transformation, have been clarified, providing significant reference value for the experimental design of pre-alloying molybdenum-silicon powders.

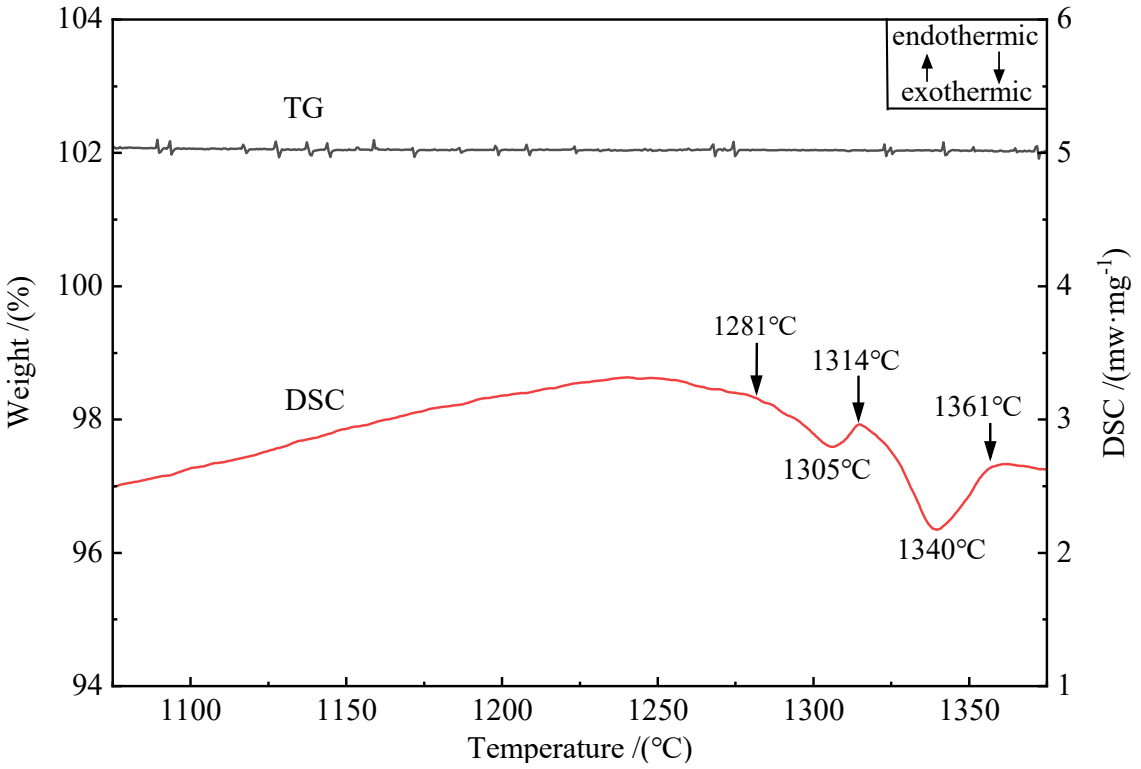

Figure 1. DSC-TG curve of a mixed powder with a Mo-Si atomic ratio of 1:9.

2.2. Preparation of Molybdenum-Silicon Alloy Powder

The molybdenum-silicon mixed powder was placed in an alumina crucible and positioned within a high-temperature vacuum tube furnace. Under high-vacuum conditions, heat treatment was carried out by holding the sample at 1200 °C, 1250 °C, 1300 °C, 1350 °C and 1400 °C for 2 h, yielding molybdenum-silicon alloyed billets subjected to different heat treatment temperatures. Furthermore, the holding time was reduced to 0.5 h and 1 h at specific temperatures to investigate the molybdenum-silicon reaction process. Finally, the alloyed billets obtained under different heat treatment conditions were ground and crushed; after ball milling, molybdenum-silicon pre-alloyed powder was obtained, with the ball milling conditions being a ball-to-powder ratio of 10:1, a duration of 20 min, and a speed of 300 r/min.

2.3. Forming and Sintering

The alloyed powders obtained at alloying temperatures of 1350 °C and 1400 °C and a holding time of 2 h were placed in graphite moulds, which were then placed in a vacuum sintering furnace for sintering. Concurrently, unalloyed molybdenum-silicon mixed powder was used as a control group and directly hot-pressed using the same process, to enable a comparative analysis of the differences in microstructural morphology and structural characteristics between the molybdenum-silicon sintered samples prepared from the two different powder raw materials. The hot-press sintering process was carried out in an argon atmosphere at a sintering temperature of 1350 °C, with a holding time of 2 h and a pressure of 35 MPa, maintaining a heating rate of 5 °C/min.

2.4. Performance Characterisation

XRD was used to determine the phase composition of the alloyed powder, with the following test parameters: Cu-Kα radiation, scanning angle 20–90°, and scanning speed 2°/min. The laser particle size analyser was employed to analyse the particle size distribution of the alloyed powder. The morphology and particle size of the experimental samples were directly observed using secondary electrons and backscattered electrons from the field-emission scanning electron microscope (SEM), whilst the composition of the phases was analysed using the point-scan mode of the energy dispersive spectrometer (EDS); the bulk density of the sintered samples was determined using the Archimedes' principle, and the ratio of the measured density to the theoretical density was calculated to characterise the material's compactness, with the results presented as a percentage.

3. Results and Discussion

3.1. Effect of Heat Treatment Conditions on Alloying

3.1.1. Effect of Heat Treatment Temperature on Alloying

The alloyed green bodies obtained at different heat treatment temperatures are shown in Figure 2. It can be observed that as the temperature rises from 1200 °C to 1400 °C, the colour of the green body gradually changes from grey-brown to grey-blue, and the powder transitions from a loose state to a compacted state, becoming increasingly hard. At 1400 °C, coarse grains are already present and there are distinct voids between the powder particles. Figure 3 shows a scanning image of the coarse grains in the molybdenum-silicon mixed powder used in the experiment and the alloyed green body after sintering at 1400 °C. EDS analysis was performed on the phases at positions 1 and 2, and the semi-quantitative results are shown in Table 1. The scanning image of the molybdenum-silicon mixed powder is shown in Figure 3a. The molybdenum powder appears as small spherical particles, whilst the silicon powder predominantly appears in agglomerated form, with some silicon particles exhibiting irregular shapes; finer-grained silicon powder, due to its higher surface energy, readily adsorbs onto the surface of the molybdenum powder. In Figure 3b, approximately circular particles (marked 1) are observed distributed on the matrix (marked 2), with some already embedded. EDS analysis revealed that position 1 corresponds to the $MoSi_2$ phase and position 2 to the Si phase; peaks associated with Mo and Si were observed at position 1. with an atomic ratio close to 0.5. Combined with the initial morphology of the molybdenum-silicon mixed powder, this indicates that the approximately spherical particles constitute the $MoSi_2$ phase. Meanwhile, the signal at position 2 corresponds to Si, confirming that the substrate is of the Si phase. It can be observed that both the $MoSi_2$ phase and the Si phase exhibit a tendency towards grain growth.

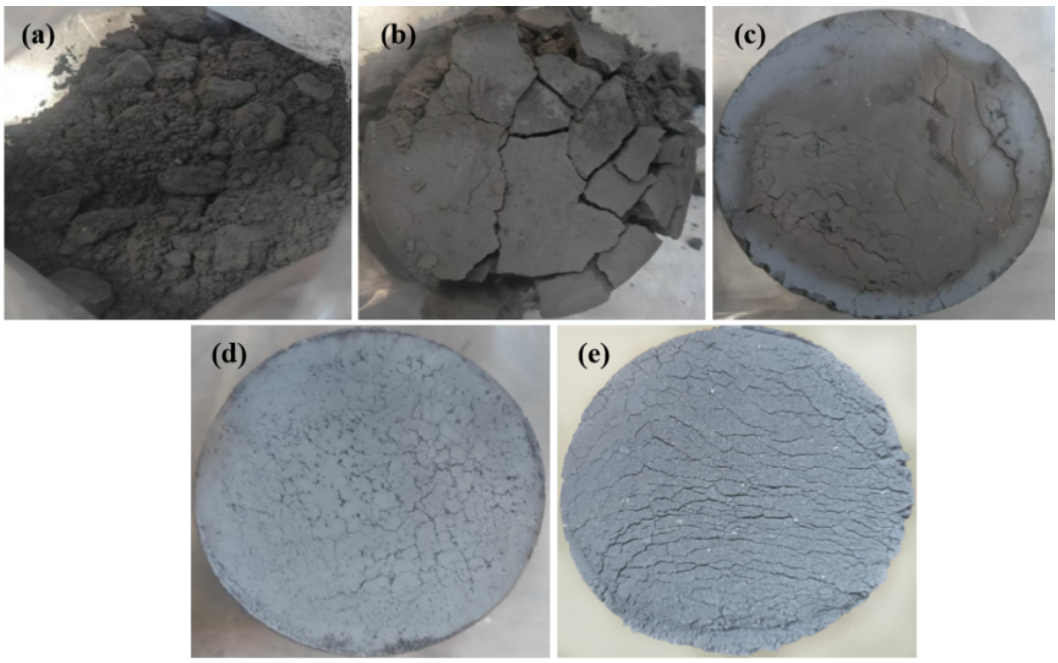

Figure 2. Mixed powder with a Mo-Si atomic ratio of 1:9 alloyed billet at 1200 °C to 1400 °C with a 2-h soak: (**a**) 1200 °C; (**b**) 1250 °C; (**c**) 1300 °C; (**d**) 1350 °C; (**e**) 1400 °C.

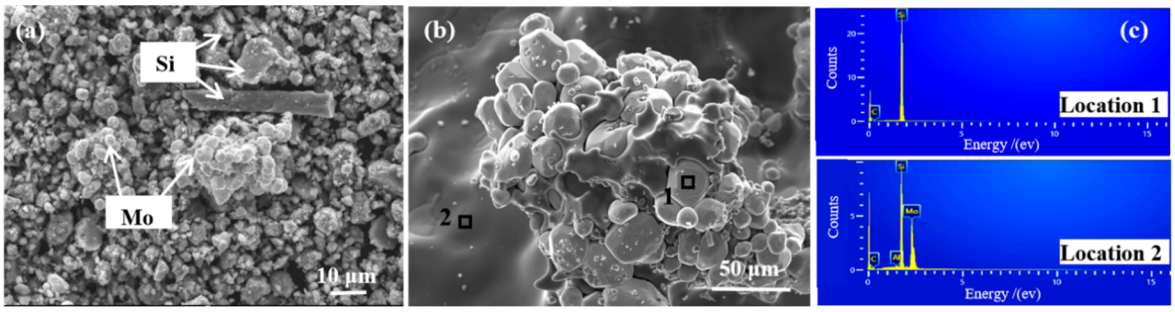

Figure 3. The state of the powder before and after heat treatment: (**a**) the mixed powder with a Mo-Si atomic ratio of 1:9; (**b**) sintered body at 1400 °C; (**c**) EDS spectrum.

Table 1. Atomic composition at positions 1 and 2.

Location	Mo Content (%)	Si Content (%)	Atomic Ratio of Mo/Si
1	33.4	66.6	1:2
2	-	100	-

Figure 4 shows the XRD patterns of various samples of the molybdenum-silicon mixture following heat treatment at different temperatures. It can be seen that at 1200 °C, the diffraction peaks for Mo and Si are clear and sharp, whilst only a faint characteristic diffraction peak of the $MoSi_3$ phase is observed at 41.3°, indicating that at this temperature the vast majority of the powder exists in its elemental state, and that the molybdenum and silicon powders have essentially not reacted; At 1250 °C, characteristic Mo_3Si peaks appear near 25.7°, 36.8°, 41.3° and 45.4°, accompanied by distinct $MoSi_2$ diffraction peaks; the molybdenum and silicon begin to react, but a significant amount of unreacted raw Mo and Si remains. As the temperature rises to 1300 °C, the intensity of the Mo diffraction peaks decreases, the diffraction intensities of the Mo_3Si and $MoSi_2$ phases increased, and as silicon gradually diffused into the molybdenum [17,18], the Mo and Mo_3Si phases gradually transformed into Mo_5Si_3 and $MoSi_2$ phases; the reaction rate of the molybdenum-silicon reaction increased, but a small amount of Mo remained; when the temperature reaches 1350 °C, the peak shapes of the $MoSi_3$ and Mo_5Si_3 phases disappear, and Mo exists entirely in the form of the $MoSi_2$ phase with an increased diffraction peak intensity, indicating that the molybdenum-silicon reaction is complete and the degree of crystallization has increased; As the temperature continues to rise, it can be seen from Figure 3 that, accompanied by the growth of Si and $MoSi_2$ grains, the relative diffraction intensities of the crystal planes of each substance undergo certain changes. Therefore, the experiments demonstrate that the molybdenum-silicon reaction is primarily a diffusion-controlled heterogeneous solid-state reaction; that is, as the temperature gradually increases, the diffusion of silicon into molybdenum gradually intensifies, and the sequence of phase formation is Mo + Si → Mo_3Si + Si → Mo_5Si_3 + Si → $MoSi_2$. Specifically, molybdenum silicide undergoes an incomplete reaction at 1200 °C, and the Mo_3Si phase begins to form; in the temperature range of 1250–1300 °C, further reaction of molybdenum silicide leads to the formation of the Mo_5Si_3 phase; the reaction of molybdenum silicide tends toward completion at 1350 °C, with only the $MoSi_2$ phase remaining. Combined with DSC test data, the exothermic peaks of the reaction are relatively concentrated, indicating a fast reaction rate and a narrow reaction range for molybdenum silicide. That is, the specific temperature ranges for the appearance and disappearance of each intermediate phase may overlap, which is consistent with the experimental observations in this study. To determine the temperature ranges for the independent phase transitions of each phase, further in-depth investigation is required. In summary, under conditions of a 2-h holding time, the optimal alloying temperature for the mixed powder with a molybdenum-silicon atomic ratio of 1:9 is 1350 °C.

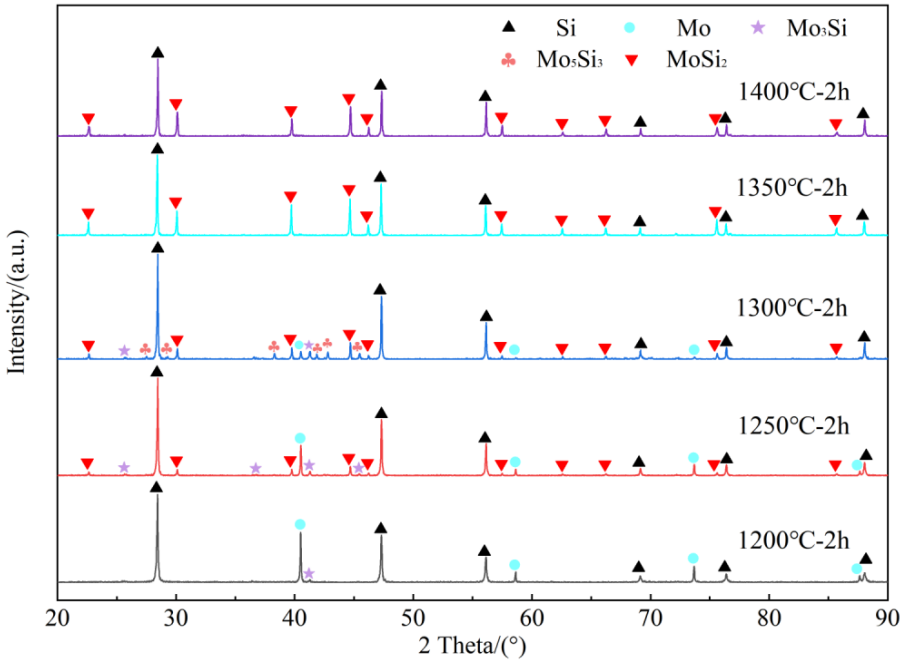

Figure 4. XRD energy spectrum of a molybdenum-silicon mixture powder with an atomic ratio of 1:9 at different heat treatment temperatures after 2 h of holding.

3.1.2. Effect of Heat Treatment Duration on Alloying

As demonstrated by the above experiments, higher temperatures result in increasingly severe agglomeration of the powder and a greater degree of densification. To reduce the degree of agglomeration, facilitate subsequent mechanical grinding and fragmentation, and thereby minimise the likelihood of impurity introduction, the holding time at 1350 °C was reduced to investigate the effect of heat treatment duration on the silicon alloying of molybdenum. Figure 5 shows the XRD diffraction patterns of the Mo-90 at.%Si mixed powder after holding at 1350 °C for 0.5 h, 1 h and 2 h. Only diffraction peaks corresponding to the Si and $MoSi_2$ phases are present; the peak shapes are complete and sharp, indicating that there is no significant change in the phase composition under different holding times. both molybdenum and silicon have reacted completely to form $MoSi_2$, and as the holding time increases, the diffraction intensity of the individual peaks of the $MoSi_2$ phase increases, the crystallinity of $MoSi_2$ gradually improves, and the interaction between molybdenum and silicon intensifies. Extending the holding time at 1350 °C enhances the crystalline properties of the powder and also makes the alloyed billet increasingly hard. The molybdenum-silicon reaction proceeds rapidly, similar to self-propagating high-temperature synthesis (SHS). The heat released by the molybdenum-silicon reaction causes a localised rise in temperature, providing the energy required for the subsequent sustained reaction. With the addition of external energy, this is akin to a chain reaction triggering an explosive reaction, thereby accelerating the reaction rate. Under room temperature conditions, disregarding phase transitions and energy transfer outside the reaction system, and assuming complete Mo-Si reaction with all heat released absorbed by substances within the system. In the reaction Mo (s) + 2 Si (s) = $MoSi_2$ (s), the enthalpy change is −131.78 kJ/mol. The temperature rise caused by the reaction is calculated using the following equation:

$$\Delta H_{298}^{\theta} = \int_{298}^{Tad} C_p dx \quad (1)$$

Where ΔH_{298}^{θ} is the standard molar reaction enthalpy, T_{ad} is the temperature that the system can reach, and C_p is the specific heat capacity at constant pressure. C_p is a function of temperature, with units of J/(mol·K). Through experimental fitting, it can be expressed by Equation (2), where a, b, c, and d are the temperature coefficients of specific heat, which are material-specific constants. The empirical parameters within a certain temperature range are shown in Table 2 below [19]. Calculations show that the temperature achievable upon reaction initiation is 1942.13 K, which is close to the theoretical adiabatic temperature of 1900 K in SHS [20]. As the silicon content increases, when the molar ratio of molybdenum to silicon is 1:9, taking into account the heat of fusion of silicon (50.208 kJ/mol), it is calculated that at a reaction temperature of 1350 °C, the local instantaneous temperature generated by the molybdenum-silicon reaction can reach the melting point of silicon, causing the silicon to soften or even melt. This increases the contact area between the molybdenum powder and the silicon powder, thereby promoting the completion of the molybdenum-silicon reaction within a shorter time.

$$C_p = a + b \times 10^{-3}T + c \times 10^{5}T^{-2} + d \times 10^{-6}T^{2} \quad (2)$$

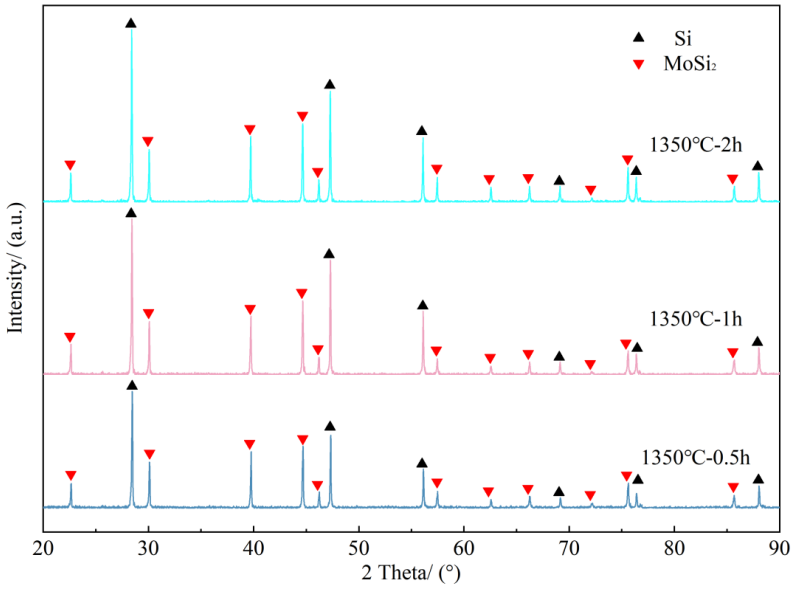

Figure 5. XRD patterns of a molybdenum-silicon mixture with an atomic ratio of 1:9 at 1350 °C for different heat treatment times.

Table 2. Empirical parameters for the relevant substance [19].

Matter	State (K)	a	b	c	d
$MoSi_2$	S (298~2303)	67.831	11.970	−6.569	-
Si	S (298~1685)	22.824	3.858	−3.540	-
	l (1685~3492)	27.196	-	-	-

3.2. The Study of the Formation Mechanism of $MoSi_2$

Gibbs free energy is a key state function in thermodynamics used to determine whether a reaction proceeds spontaneously under isothermal and isobaric conditions; a reaction proceeds spontaneously when the change in Gibbs free energy ($\Delta_r G$) is less than zero. When temperature variations are small, the change in Gibbs free energy under non-standard conditions for various heterogeneous solid-state reactions in the Mo-Si system can be treated linearly. According to the Van't Hoff isothermal equation, the following equation (3) can be derived [17]:

$$\Delta_r G = \Delta_r G^{\theta} = A + BT \quad (3)$$

where: $\Delta_r G$ is the reaction Gibbs free energy; T is the temperature; A and B are the relevant correction coefficients. In the Mo-Si binary system, with a total reactant amount of 1 mol, the following reaction equations apply:

$$3/4\ Mo\ (s) + 1/4\ Si\ (s) = 1/4\ Mo_3Si\ (s) \quad (4)$$

$$5/8\ Mo\ (s) + 3/8\ Si\ (s) = 1/8\ Mo5Si_3\ (s) \quad (5)$$

$$1/3\ Mo\ (s) + 2/3\ Si\ (s) = 1/3\ MoSi_2\ (s) \quad (6)$$

$$5/9\ Mo_3Si\ (s) + 4/9\ Si\ (s) = 1/3\ Mo_5Si_3\ (s) \quad (7)$$

$$1/6\ Mo_3Si\ (s) + 5/6\ Si\ (s) = 1/2\ MoSi_2\ (s) \quad (8)$$

$$1/8\ Mo_5Si_3\ (s) + 7/8\ Si\ (s) = 5/8\ MoSi_2\ (s) \quad (9)$$

Using Equation (3), within a certain temperature range, the Gibbs free energy changes for each reaction between 1000 °C and 1400 °C can be calculated based on the thermodynamic parameters of relevant silicides in the Mo-Si system reported in Reference [19]. For reactions (4) to (6), the values of A and B are shown in Table 3. Through a linear combination of the reactions, the Gibbs free energy expressions for other reactions within the Mo-Si system can be obtained, and $\Delta_r G$ for each of the above reactions at different temperatures can be calculated. This further yields the relationship between Gibbs free energy and temperature for the Mo-Si reaction system; the calculation results are shown in Figure 6.

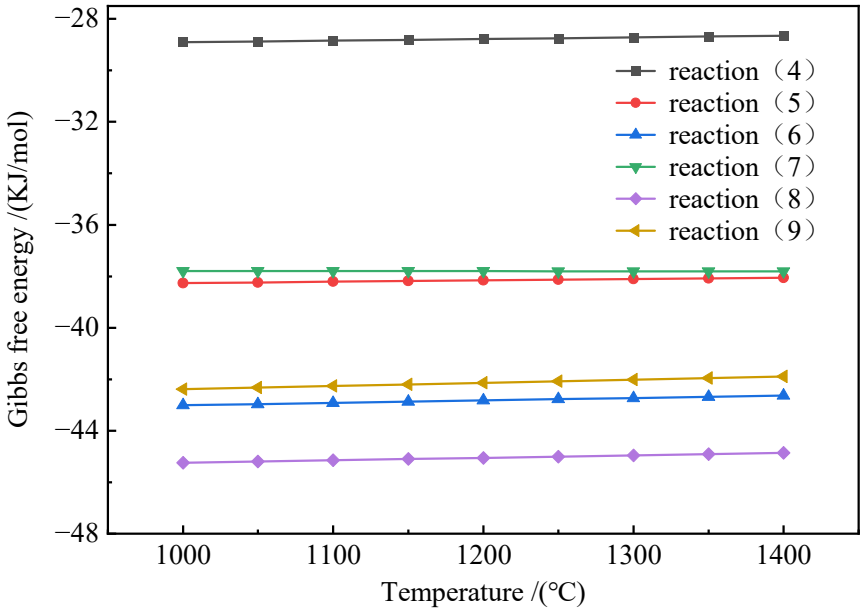

Figure 6. Gibbs free energy versus temperature plot for the Mo-Si reaction system.

Table 3. The values of parameters A and B in the relationship $\Delta_r G = A + BT$ for reactions (4) to (6) [19].

Reaction	A/(J·mol^{-1})	B/(J·mol^{-1})	Operating Temperature Range
Reaction (4)	−118 800	2.5	25 °C~1 412 °C
Reaction (5)	−311 300	4.1	25 °C~1 412 °C
Reaction (6)	−132 600	2.8	25 °C~1 412 °C

From a purely thermodynamic perspective, within the temperature range of 1200 °C to 1400 °C, the Gibbs free energy of all reactions in the Mo-Si binary system is negative, meaning they all proceed spontaneously. Furthermore, according to the Gibbs free energy criterion, the smaller the $\Delta_r G^{\theta}$, the greater the tendency for the reaction to proceed spontaneously. Upon comprehensive comparison, reaction (4) is at the end of the reaction sequence, indicating that this reaction has the lowest tendency to occur in the Mo-Si reaction system, whilst reaction (8) is the most likely to occur. However, experiments show that the first reaction to occur is reaction (4), with Mo_3Si being formed first. In chemical reactions, thermodynamics provides theoretical guidance; it reflects the tendency for substances to transform into one another and indicates the direction of the reaction. However, whether a reaction occurs and its rate depend not only on thermodynamic conditions but also, to a large extent, on the kinetic conditions of the reaction. In heterogeneous solid-state reactions, with a fixed holding time, Si gradually diffuses into Mo at a given temperature, initially forming Mo_3Si; as the temperature rises, the diffusion capacity of Si increases and the diffusion depth grows. Since the $\Delta_r G$ for reaction (4) is the highest, indicating that the Mo_3Si phase is unstable, Mo_3Si and Si react further, transforming into products with higher Si content. simultaneously, as the reaction enthalpies of reactions (5) and (7) become similar, and given the greater reactivity of reaction (6) within the Si-enriched Mo-Si binary system, Mo and Si can react directly to form Mo_5Si_3 and $MoSi_2$; When the temperature rises to 1350 °C, a series of reactions from reactions (4) to (9) occur; the molybdenum silicide reacts completely, and the reaction releases a large amount of heat which provides the activation energy required for the reactions between the substances, thereby facilitating the reaction process of the system.

To investigate the effectiveness of the "powder pre-alloying + hot-press sintering" process in improving the micro-structural uniformity of target blanks, this study employed a mixed powder with a molybdenum-to-silicon atomic ratio of 1:9 as raw material for direct hot-press sintering, in order to obtain comparable control experimental data. The study found that large-particle-size Mo particles are prone to exhibiting a layered structure. EDS was used to further characterize the distribution of Mo and Si elements within this layered structure, with the results shown in Figure 7. Due to differences in contrast, the large-particle-size Mo particles in Figure 7a exhibit a distinct three-layer structure: the outermost layer consists of $MoSi_2$; the middle layer is a transition phase; and the core layer consists of unreacted Mo. For Mo particles, as one moves from the exterior toward the interior, the Mo content gradually increases while the Si content gradually decreases. This confirms that Si diffusion into the Mo interior is the dominant mechanism of the in-situ Mo-Si reaction, and the phase transformation follows a pattern of gradual transition from a low-Si phase to a high-Si phase. Combining the aforementioned XRD analysis with thermodynamic calculations indicates that, as Si diffuses into Mo, the molybdenum-silicon reaction follows a stepwise phase transformation pathway: "Mo + Si → Mo_3Si + Si → Mo_5Si_3 + Si → $MoSi_2$".

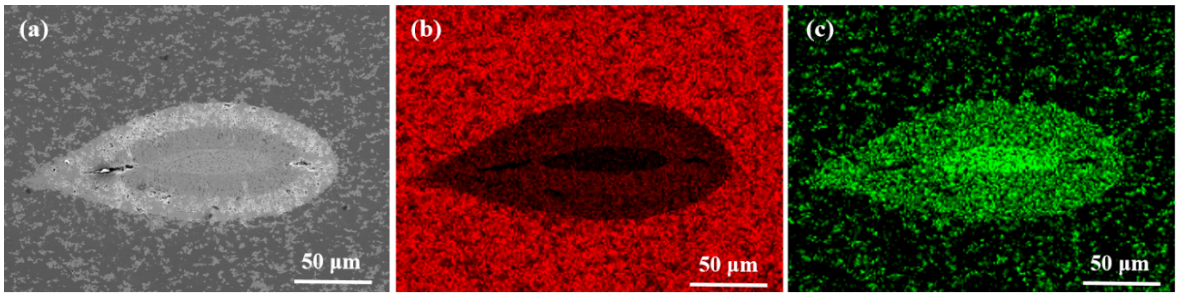

Figure 7. BSE image of a large Mo particle and its corresponding elemental maps: (**a**) BSE image; (**b**) Si elemental map; (**c**) Mo elemental map.

3.3. Effect of Mechanical Ball Milling on the Morphology of Molybdenum-Silicon Alloy Powder

Figure 8 shows SEM images of MoSi alloy powder obtained after pre-alloying and ball milling of mixed powders held at different heat treatment temperatures for 2 h. Figure 8a,c are the secondary electron images of the powder after crushing of the alloyed billets obtained after heat treatment at 1350 °C and 1400 °C, respectively. Figure 8b,d are the corresponding backscattered electron images. In the Figure 8b,d, combined with EDS spectra, it is clear that the grey areas correspond to Si, whilst the bright areas correspond to Mo or MoSi compounds. In

conjunction with the XRD diffraction patterns, the reaction between molybdenum and silicon is complete at 1350 °C and 1400 °C, leaving only the Si phase and the $MoSi_2$ phase; the green body is hard and dense. At 1350 °C, following preliminary mechanical crushing, both Si and $MoSi_2$ exhibit varying particle sizes, with Si predominantly appearing in rod-like and columnar forms, and some agglomeration naturally occurring. And the $MoSi_2$ phase exhibits significant plastic deformation and irregular shapes. During ball milling, the grinding balls collide with one another, generating high-energy impacts. The resulting kinetic energy is transferred to the alloy powder, causing the powder particles to undergo plastic deformation under the continuous impact and fragmentation of the grinding media, which in turn increases the defect density within the particles [21]. At the same time, as the particles are continuously refined, their specific surface area gradually increases, thereby enhancing the surface activity of the powder. Because ball milling introduces a high density of defects, the powder enters a high-energy non-equilibrium state. During subsequent hot pressing, this reduces the atomic diffusion energy barrier during subsequent hot pressing and increases the sintering driving force, facilitating atomic diffusion and densification processes, and thereby effectively improving the sintering activity of the powder. After the alloyed billets at 1400 °C have been crushed, the particles are refined to varying degrees. The grinding balls continuously impact the alloy powder; this mechanical force not only breaks the powder but also causes it to deform. Furthermore, the non-uniformity of energy transfer leads to varying degrees of deformation in the powder, resulting in particles of differing sizes. The silicon appears as irregular lumps, whilst the $MoSi_2$ particles are approximately spherical, making them more difficult to crush.

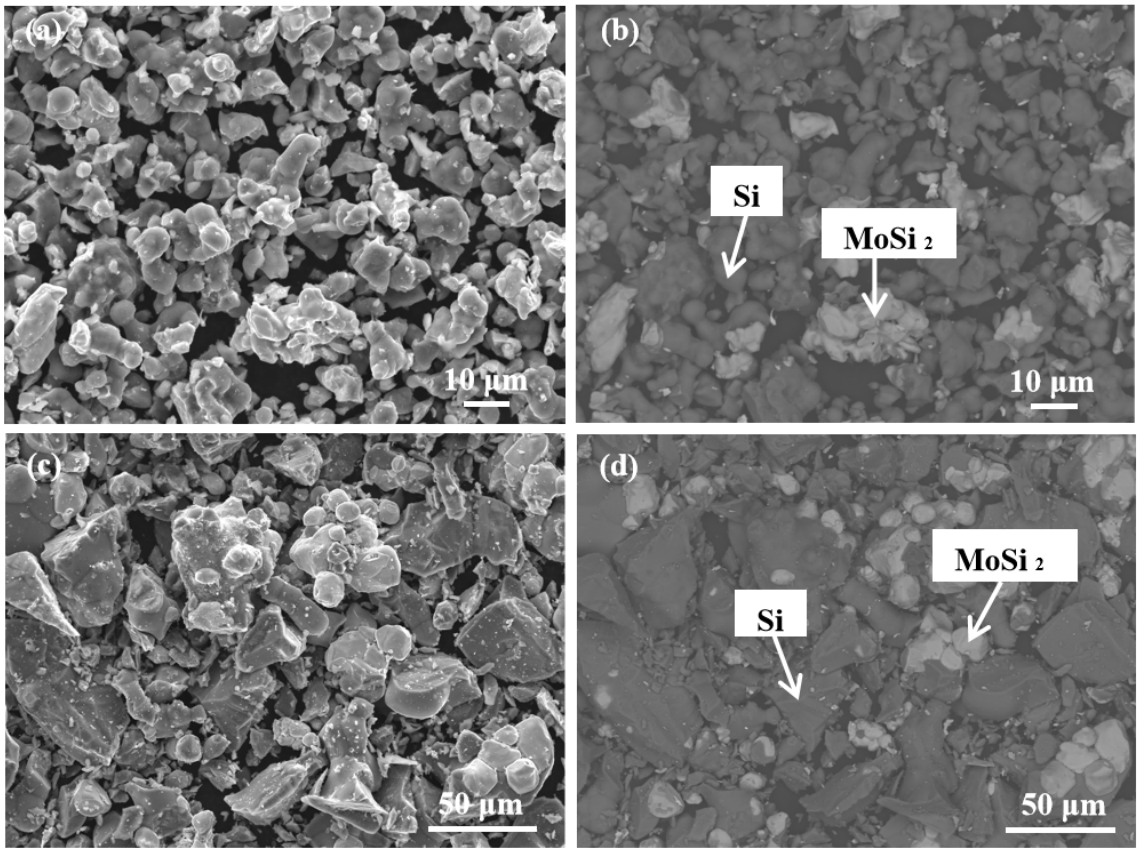

Figure 8. Scanning electron microscope images of Mo-Si pre-alloyed and comminuted alloy powder at different heat treatment temperatures with a 2-h soak period: (**a**,**b**) 1350 °C; (**c**,**d**) 1400 °C.

Combining laser particle size analysis with powder particle size characterisation, Equation (10) below describes the width of the particle size distribution, D_δ:

$$D_\delta = (D_{90} - D_{10})/D_{50} \quad (10)$$

where D_{10}, D_{50} and D_{90} represent the particle sizes corresponding to 10%, 50% and 90% of the volume of the powder, respectively. Figure 9 shows the particle size distribution of molybdenum-silicon alloy powder following comminution under different heat treatment conditions. It can be observed that, following molybdenum-silicon alloying and mechanical comminution under various heat treatment conditions, the alloy powder exhibits a unimodal distribution. As the degree of sintering of the alloyed billets decreases, the refinement of the powder

becomes more pronounced; at 1350 °C for 2 h, D_δ remains at approximately 1.2, the particle size distribution tends to narrow, and ball milling has a marked improving effect on the particle size distribution. In summary, as the temperature rises, the billets become increasingly hard, making crushing more difficult. Under virtually identical crushing conditions, the refinement of the powder occurs more slowly. Furthermore, the Si-$MoSi_2$ mixture belongs to a brittle-brittle system. During the initial crushing stage, the brittle silicon phase is more prone to fracture, undergoing slight plastic deformation and transitioning from irregular large lumps to rod-like shapes, whilst $MoSi_2$ is more susceptible to deformation, exhibiting significant plastic deformation and gradually transforming from a spherical shape into an irregular form.

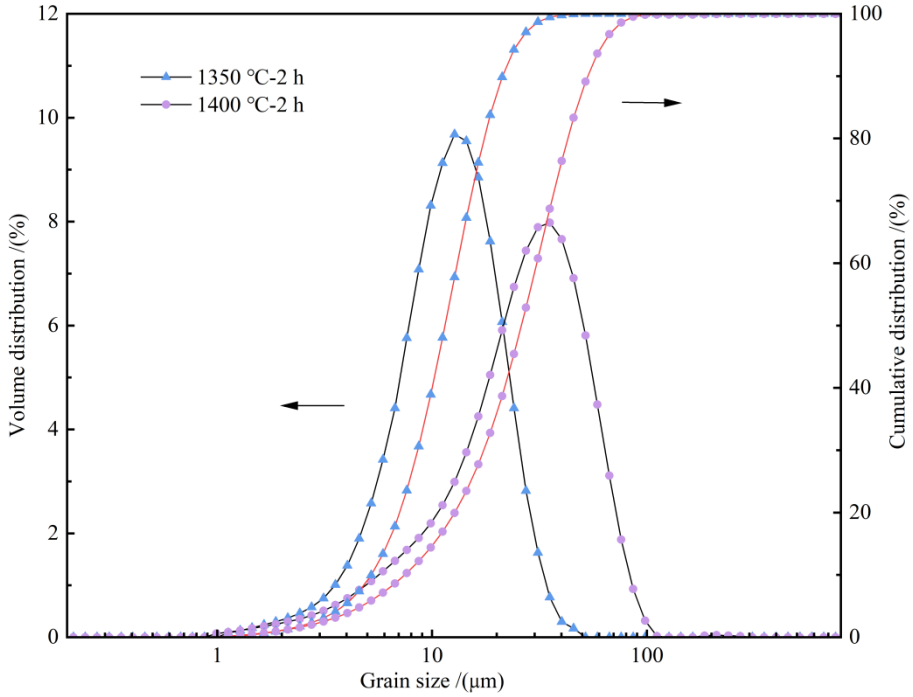

Figure 9. Particle size distribution of crushed molybdenum-silicon alloy under different heat treatment conditions.

3.4. Preparation of Molybdenum-Silicon Alloy Target Materials

Using hot-pressed targets made from molybdenum-silicon mixed powder as a control, the effect of alloyed powder on the microstructure of molybdenum-silicon targets after ball milling was observed. Figure 10 below shows SEM images and cross-sectional views of hot-pressed samples of molybdenum-silicon alloy powder and molybdenum-silicon mixed powder prepared after holding at different heat treatment temperatures for 2 h, where the dark phase represents the Si phase and the light-coloured regions represent the $MoSi_2$ phase. In Figure 10c, the $MoSi_2$ phase is distributed within the Si matrix and exhibits agglomeration. The localised temperature rise caused by the significant heat released during the Mo-Si reaction at high temperatures and under hot-pressing conditions accelerated atomic diffusion. The rapid growth of the sintering neck prevented gases from escaping in time, resulting in a high number of pores within the $MoSi_2$ phase. Combined with the cross-sectional morphology, it can be seen that the sintering is relatively dense; most fracture surfaces are flat and bright, exhibiting either large-area or granular features. The fracture presents a mixed mode of intergranular and transgranular fracture, wherein the silicon phase exhibits a transgranular fracture mode and is relatively brittle, whilst the $MoSi_2$ phase, with its granular morphology, exhibits intergranular fracture. In the scanning image of the alloyed powder sample at 1400 °C, there are generally many voids and cracks in the $MoSi_2$ phase, indicating insufficient sintering; furthermore, numerous cylindrical interconnected and circular closed pores were observed on the fracture surface. The pore size is relatively large, the density is low, and the material is in the mid-to-late stage of sintering. This is because, following preliminary comminution, the alloy powder particles are irregular in shape and coarse; particle reorganisation is significantly impeded and surface energy is low, requiring higher energy to drive atomic diffusion, resulting in insufficient sintering. In contrast, the scanning image of the alloyed powder sample at 1350 °C shows the $MoSi_2$ phase uniformly distributed across the silicon matrix, with a small number of voids distributed within the Si phase. Combined with the fracture surface image, which reveals circular voids, the sintering is not fully complete; sintering activity can be improved by further comminution to refine the particle size. As the powder is relatively fine following preliminary comminution, the degree of densification has increased to 99.5%.

Compared to the hot-pressed samples of the molybdenum-silicon mixed powder, the uniformity of the microstructure has also been improved to some extent.

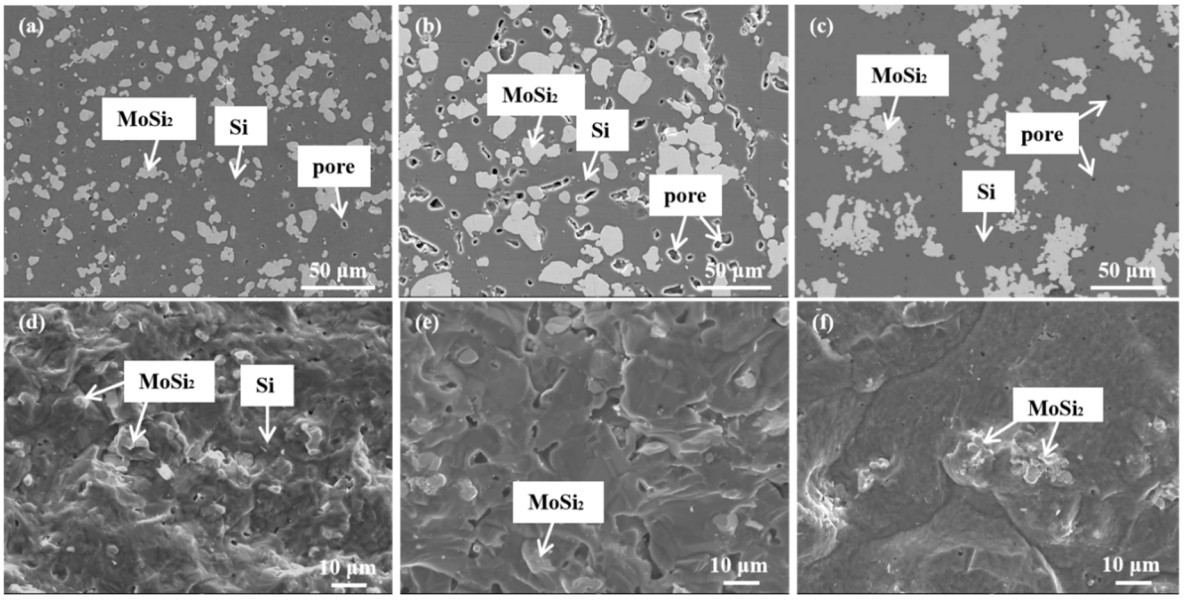

Figure 10. SEM images and fracture surface morphology of MoSi samples produced by hot pressing different raw material powders: (**a**,**d**) alloy powder heat-treated at 1350 °C; (**b**,**e**) alloy powder heat-treated at 1400 °C; (**c**,**f**) MoSi sample produced by direct hot-press sintering of a Mo-Si mixed powder.

4. Conclusions

This study primarily involved the preparation of molybdenum-silicon alloy powder with fine, uniform grains by optimizing the heat treatment process and ball milling of molybdenum-silicon mixed powder. This powder was then subjected to hot-press sintering to produce high-density molybdenum-silicon targets with a uniform micro-structure. The main conclusions of this study are outlined below.

(1) When synthesising molybdenum-silicon alloy powder composed of $MoSi_2$ and Si phases from a mixed powder with an atomic ratio of Mo:Si = 1:9, the optimal heat treatment temperature is 1350 °C, with a holding time of 2 h. In the Mo-Si binary system, Mo_3Si forms initially; as the reaction temperature rises, Si gradually diffuses into Mo, and the sequence of phase formation is $Mo + Si \rightarrow Mo_3Si + Si \rightarrow Mo_5Si_3 + Si \rightarrow MoSi_2$.

(2) Si-$MoSi_2$ alloy powder belongs to a brittle-brittle system, where the Si phase is more prone to fracturing, evolving from irregular large lumps to rod-like shapes, whilst the $MoSi_2$ phase exhibits distinct plastic deformation. Under identical ball-milling conditions, as the degree of powder consolidation decreases, the refinement of the alloyed powder particle size becomes increasingly pronounced, whilst simultaneously significantly enhancing its sintering activity, which is conducive to the densification of molybdenum-silicon target materials.

(3) By optimising the alloying parameters and integrating the subsequent comminution and sintering processes, molybdenum-silicon target materials with a relative density of 99.5% were successfully produced. Compared with the direct hot-pressing process, the uniformity of the micro-structure was effectively improved.

Research has shown that high density in target materials implies low internal porosity and a uniform micro-structure. During the sputtering process, this not only increases sputtering rates and extends the service life of the target but also effectively suppresses gas release and particle sputtering, thereby reducing arc discharge and preventing film defects; the uniformity of target's micro-structure helps improve sputtering rates and film thickness uniformity. However, due to experimental limitations, this study was unable to complete sputtering deposition and related performance characterization of the prepared molybdenum-silicon targets with uniform micro-structure, and thus could not definitively evaluate the target quality through systematic sputtering characterization. Future research will focus on optimizing the preparation process for high-purity, micro-structurally uniform, and highly dense molybdenum-silicon targets, as well as characterizing their sputtering deposition performance. The goal is to establish the correlation mechanism between the target's micro-structure and sputtering performance to verify its suitability for photo-mask applications.

Author Contributions

X.G.: data curation, writing—original draft preparation; N.F.: methodology, supervision, writing—reviewing and editing; Z.D.: methodology, resources; Q.J.: resources, experimental design, and data analysis; Y.R.: writing—reviewing and editing; J.H.: methodology, resources. All authors have read and agreed to the published version of the manuscript.

Funding

This research received no external funding.

Institutional Review Board Statement

Not applicable.

Informed Consent Statement

Not applicable.

Conflicts of Interest

N.F., Z.D., Q.J., Y.R., and J.H. are employees of Grikin Advanced Materials Co., Ltd. X.G. is a graduate student trained by Grikin Advanced Materials Co., Ltd. The authors declare that these affiliations are the only potential conflicts of interest related to this work and that they did not influence the design, execution, analysis, interpretation, or presentation of the research.

Use of AI and AI-Assisted Technologies

No AI tools were utilized for this paper.

References

1. Pratap, S.; Jauhar, S.K.; Gunasekaran, A.; et al. Optimizing the IoT and Big Data Embedded Smart Supply Chains for Sustainable Performance. *Comput. Ind. Eng.* **2024**, *187*, 109828.
2. Li, S. Analysis of the Prospect of New Energy and Low-Altitude Economy Industry Combination under the Background of Low-Carbon Economy. *Acad. J. Bus. Manag.* **2024**, *6*, 179–183.
3. French, R.H.; Tran, H.V. Immersion Lithography: Photomask and Wafer-Level Materials. *Annu. Rev. Mater. Res.* **2009**, *39*, 93–126.
4. Cao, K.W.; Wu, Y.R.; Zhang, J.H.; et al. Current Status and Development Direction of Mask Standards. *Stand. Sci.* **2022**, *S1*, 91–95. https://doi.org/10.3969/j.issn.1674-5698.2022.z1.016. (In Chinese)
5. Osipov, A.A.; Gagaeva, A.E.; Speshilova, A.B.; et al. Development of Controlled Nanosphere Lithography Technology. *Sci. Rep.* **2023**, *13*, 3350.
6. Shapiro, S.; Tan, S.K.; Maeng, J.Y.; et al. Application of KrF PSM in ArF Photolithography Processing. In Proceedings of SPIE Photomask Technology and Extreme Ultraviolet Lithography, Monterey, CA, USA, 29 September–3 October 2024; pp. 517–528.
7. Zhang, S.J.; Shen, M.H.; Xu, Y.; et al. Performance Comparison between Attenuated PSM and Opaque MoSi on Glass (OMOG) Mask in Sub-32 nm Litho Process. *ECS Trans.* **2012**, *44*, 249–256.
8. Carcia, P.F.; French, R.H.; Sharp, K.G.; et al. Materials Screening for Attenuating Embedded Phase-Shift Photoblanks for DUV and 193-nm Photolithography. In Proceedings of the 16th Annual BACUS Symposium on Photomask Technology and Management, Redwood City, CA, USA, 18–20 September 1996; pp. 255–263.
9. Wu, Q.; Hu, H.Y.; He, W.M.; et al. *Photolithography Process Near the Diffraction Limit*; Tsinghua University Press: Beijing, China, 2020; pp. 285–290. (In Chinese)
10. Ji, P. Simulation of Plasma Property Distribution and Sputtering Characteristics of Targets in Magnetron Sputtering. Master's Thesis, Xi'an University of Technology, Xi'an, China, 2024. (In Chinese)
11. He, J.J.; He, X.; Xiong, X.D.; et al. Research Status of High Purity Metals and High Performance Sputtering Target Used in Integrated Circuit. *Adv. Mater. Ind.* **2015**, *17*, 47–52. (In Chinese)
12. Jia, G.B.; Feng, Y.N.; Jia, Y. Manufacture, Application and Development of Refractory Metal Target Used on Magnetron Sputtering. *Met. Funct. Mater.* **2016**, *23*, 48–52. (In Chinese)
13. Li, J.; Fu, Z.; Wei, L.; et al. Characterization of Mo-6Ta Alloy Targets and Its Magnetron Sputtering Deposited Thin Film. *Int. J. Refract. Met. Hard Mater.* **2022**, *103*, 105770.

14. Huang, Z.M.; Wang, D.Z.; Wu, Z.Z.; et al. Preparation Technology of Tungsten Silicide Alloys Used for Sputtering Target. *Powder Metall. Technol.* **2021**, *39*, 445–451. (In Chinese)
15. Peng, X.M.; Xia, C.Q.; Liu, Y.Y.; et al. Surface Molybdenizing on Titanium by Halide-Activated Pack Cementation. *Surf. Coat. Technol.* **2009**, *203*, 3306–3311.
16. Honma, T.; Tatami, J. Effects of Molybdenum Volume Fraction and Silica Molybdenum Particle-Size Ratio on Relative Bulk Density and Electrical Conductivity of Silica-Molybdenum Composites Fabricated by Spark Plasma Sintering. *J. Mater. Sci.* **2014**, *49*, 5878–5884.
17. Lambert, D.S.; Lennon, A.; Burr, P.A. Diffusion Mechanisms of Mo Contamination in Si. *Phys. Rev. Mater.* **2020**, *4*, 025403.
18. Qiu, M.F.; Cui, C.X.; Li, Y.; et al. Microscopic Mechanism for the Interfacial Diffusion in Mo/Si Multilayers from Molecular Dynamics Simulations. *J. Mater. Eng. Perform.* **2026**, *35*, 4797–4807.
19. Liang, Y.J.; Che, Y.C. *Handbook of Thermodynamic Data for Inorganic Compounds*; Northeast University Press: Shenyang, China, 1993; p. 466. (In Chinese)
20. Deevi, S.C. Self-Propagating High-Temperature Synthesis of Molybdenum Disilicide. *J. Mater. Sci.* **1991**, *26*, 3343–3353. https://doi.org/10.1007/bf01124683.
21. Sameezadeh, M.; Farhangi, H.; Emamy, M. Structural and Morphological Evaluation of Nano-Sized $MoSi_2$ Powder Produced by Mechanical Milling. *Int. J. Mod. Phys. Conf. Ser.* **2012**, *5*, 464–471.